# Shuttle-effect-free sodium–sulfur batteries derived from a Tröger's base polymer of intrinsic microporosity

Journal of Power Sources 513 (2021) 230539

Contents lists available at ScienceDirect

Journal of Power Sources

journal homepage: www.elsevier.com/locate/jpowsour

# Shuttle-effect-free sodium–sulfur batteries derived from a Tröger's base polymer of intrinsic microporosity

Jun Woo Jeon [a,1], Dong-Min Kim [b,1], Jinyoung Lee [a], Min Su Kim [a], Min Ho Jeon [a], Richard Malpass-Evans [c], Neil B. McKeown [c], Kyu Tae Lee [b,**], Byoung Gak Kim [a,d,*]

[a] Advanced Materials Division, Korea Research Institute of Chemical Technology (KRICT), 141 Gajeong-ro, Yuseong-gu, Daejeon, 34114, Republic of Korea
[b] School of Chemical and Biological Engineering, Institute of Chemical Processes, Seoul National University, 1, Gwanak-ro, Gwanak-gu, Seoul, 08826, Republic of Korea
[c] EaStChem School of Chemistry, University of Edinburgh, Edinburgh, UK
[d] Department of Chemical Convergence Materials, University of Science and Technology, 217 Gajeong-ro, Yuseoung-gu, Daejeon, 34113, Republic of Korea

## HIGHLIGHTS

- PIM-EA-TB based carbon-sulfur composites is used for shuttle free Na–S batteries.
- The carbon-sulfur composites are prepared through the one step heat treatment.
- This is based on the synergetic effect of physical confinement and covalent bonding.
- The composites show a high reversible capacity of ~500 mA h $g^{-1}$ over 350 cycles.
- The composites demonstrate a high coulombic efficiency of ~100% over 350 cycles.

## ARTICLE INFO

*Keywords:*
Polymer of intrinsic microporosity
Na–S batteries
Tröger's base
Carbon–sulfur composite
Shuttle effect free batteries

## ABSTRACT

Room-temperature sodium–sulfur (RT Na–S) batteries have recently gained attention as next-generation energy storage devices owing to their low cost, the abundance of sodium, and the high theoretical capacity of sulfur. However, the notorious shuttle effect, caused by the dissolution of intermediate polysulfides during cycling, limits the long-term performance of Na–S batteries. In this study, intrinsically microporous Tröger's base based polymer (PIM-EA-TB)-based carbon–sulfur composites are prepared for shuttle-effect-free RT Na–S batteries by utilizing the combination of physical confinement and covalent bonding in a single material. The composites demonstrate excellent electrochemical performance, including a negligible capacity fading over 350 cycles and a high coulombic efficiency of approximately greater than 99%.

## 1. Introduction

Room-temperature sodium–sulfur (RT Na–S) batteries have recently attracted interest as one of the most promising next-generation energy storage devices because of their low cost, the earth-abundance of sodium, and the high theoretical capacity of 1675 mA h $g^{-1}$ of sulfur [1–5]. However, the notorious shuttle effect, caused by the dissolution of intermediate polysulfides during cycling, limits the long-term performance of Na–S batteries [1,2]. To overcome this shuttle effect and improve the performance of RT Na–S batteries, various approaches have been proposed, such as the use of interlayers, electrolyte additives, binders, and the development of novel cathode materials [6–15].

Among these approaches, much effort has been devoted to developing novel cathode materials to improve the performance of RT Na–S batteries. Carbonaceous materials are widely used as hosts for these cathode materials because of the insulating nature of sulfur with a conductivity of $5 \times 10^{-30}$ S $cm^{-1}$ [16,17]. To realize shuttle-effect-free RT Na–S batteries, various strategies have been investigated, with the

* Corresponding author. Advanced Materials Division, Korea Research Institute of Chemical Technology (KRICT), 141 Gajeong-ro, Yuseong-gu, Daejeon, 34114, Republic of Korea.
** Corresponding author. School of Chemical and Biological Engineering, Institute of Chemical Processes, Seoul National University, 1, Gwanak-ro, Gwanak-gu, Seoul, 08826, Republic of Korea.
*E-mail addresses:* ktlee@snu.ac.kr (K.T. Lee), bgkim@krict.re.kr (B.G. Kim).
[1] These authors contributed equally to this work.

https://doi.org/10.1016/j.jpowsour.2021.230539
Received 12 July 2021; Received in revised form 31 August 2021; Accepted 14 September 2021
Available online 25 September 2021

physical confinement and covalent bonding approaches being considered effective [2,18]. First, microporous materials can confine both sulfur and intermediate polysulfides in their micropores. For instance, small sulfur molecules, which are physically confined in micropores, cannot be dissolved into electrolytes owing to their space constraints [19]. Second, covalent bonding between the sulfur and carbon atoms could prevent the sulfur molecules from being dissolved out of the matrix. Specifically, polyarcrylonitrile (PAN)-derived carbon–sulfur composites comprising covalently bound sulfur have exhibited excellent electrochemical performance over 500 cycles [20].

As one of the successful examples of materials for preventing shuttle effects, we recently reported that polymer of intrinsic microporosity (PIM-1)-based carbon–sulfur composites demonstrated excellent electrochemical performance, including a negligible capacity fading over 250 cycles and a high coulombic efficiency greater than 99% [21]. Their unprecedented performance is due to their unique structure and related properties of the precursor polymer PIM-1, such as microporosity and the presence of the functional groups. Specifically, these traits are attributed to their ladder-like structures with contorted moieties of PIM-1, which leads to the formation of many micropores and a high surface area (>800 $m^2\ g^{-1}$) [22]. Benefiting from these features of PIM-1, the resulting PIM-1-based carbon–sulfur composites operated without the shuttle effect by combining two different concepts—namely, physical confinement and covalent bonding—in a single material. More importantly, carbon–sulfur composites have demonstrated no significant capacity fading in carbonate-based electrolytes without additives such as $LiNO_3$ to suppress the shuttle effect, although carbonate electrolytes are known to be reactive with the polysulfide, which leads to side reactions in metal–sulfur batteries [2,23,24]. Therefore, as the PIM-based carbon–sulfur composites can operate in carbonate electrolytes without additives, the combination of the two above-mentioned successful strategies using a PIM can be regarded as a promising approach to fundamentally inhibit the side reactions of sodium polysulfide.

Designing novel PIM-based carbon–sulfur composites can potentially be a good approach for developing shuttle-effect-free Na–S batteries. In particular, PIMs with a higher free volume can be used as good host matrices because they can contain more sulfur molecules than PIM-1-based carbon–sulfur composites. To date, a wide range of intrinsically microporous polymers derived from a diverse range of structural units and polymerization reactions have been synthesized [25–28]. Among them, Tröger's base (TB) polymers are attractive owing to their ease of synthesis and enhanced porosity, which can be attributed to the rigidity of the bridged bicyclic structure of the TB unit.

In this work, PIM-EA-TB-based carbon–sulfur composites were prepared for shuttle-free RT Na–S batteries. PIM-EA-TB has a higher specific surface area (>1000 $m^2\ g^{-1}$) than that of PIM-1. PIM-EA-TB was selected because its two bridged bicyclic components, namely ethanoanthracene (EA) and TB, are more rigid than the spirobisindane (SBI) and benzodioxane components of PIM-1, resulting in a higher free volume and surface area [26]. Thus, we anticipated that PIM-EA-TB could provide more space to store sulfur molecules in the active cathode materials. Moreover, we confirmed that the prepared PIM-EA-TB carbon–sulfur composite can operate without generating the shuttle effect, owing to the synergetic effect of both physical confinement and covalent bonding, as observed in PIM-1-based carbon–sulfur composites.

## 2. Experimental

### 2.1. Synthesis

#### 2.1.1. Preparation of carbonized PIM-EA-TB–sulfur composites (cPIMS-EA-TB)

PIM-EA-TB was synthesized as described previously [29]. The PIM-EA-TB-based carbon–sulfur composites were synthesized via a one-step heating process reported previously. First, ground PIM-EA-TB powder and elemental sulfur (w/w = 1:5) were mixed uniformly. The mixture was then transferred into an alumina boat and heated in a tube furnace under an inert atmosphere ($N_2$ flow, 100 cc $min^{-1}$) at a heating rate of 5 °C $min^{-1}$. Specifically, sulfur molecules were impregnated into the free volume of the PIM-EA-TB powder by heating the mixture at 155 °C for 2 h. Subsequently, the PIM-EA-TB carbon–sulfur composites were prepared by heating at 600 °C for 3 h. For comparison, a series of cPIMS samples were prepared using PIM-SBI-TB under the same conditions. Additionally, screening tests—performed to observe the changes in elemental composition by varying the final temperature and the samples—were denoted as cPIMS-X, where X is the applied final temperature (see Table S2). For instance, cPIMS-EA-TB-600 was prepared at a final temperature of 600 °C.

### 2.2. Characterization

The morphology of cPIMS-EA-TB-600 was observed via field emission scanning electron microscopy (FE-SEM, Carl Zeiss, SigmaHD) and high-resolution transmission electron microscopy (HR-TEM). Field emission transmission electron microscopy (FE-TEM) and energy-dispersive X-ray spectroscopy (EDXS) were performed for microstructural characterization and elemental mapping, respectively. Solid-state CP-MAS $^{13}C$ NMR spectra were collected at room temperature using a solid 400 MHz NB NMR at a MAS rate of 20 kHz, contact time of 5 ms, and frequency of 100 MHz for $^{13}C$ NMR. The Raman spectra of the cPIM-EA-TB-600 and cPIMS-EA-TB-600 samples were obtained using a Lab-RAM Aramis Raman spectrometer (Horiba Jobin Yvon) equipped with a 514 nm Ar-ion laser, and elemental analyses were performed using a Thermo Scientific FLASH EA-2000 organic elemental analyzer. Thermogravimetric analysis (TGA) was performed using a Pyris 1 TGA thermogravimetric analyzer (PerkinElmer). Each sample was heated from ambient temperature to 800 °C at a heating rate of 10 °C $min^{-1}$ under $N_2$ flow. The X-ray diffraction (XRD) pattern of each polymer was collected on a Rigaku Ultima IV diffractometer equipped with a graphite monochromator and Cu Kα radiation (λ = 1.5406 Å). The 2$\theta$ scanning range was 10–70° with a scanning speed of 3° $min^{-1}$. The pore characteristics such as the surface area and total pore volume of PIM-EA-TB, cPIM-EA-TB-600, and cPIMS-EA-TB-600 were calculated using a Micromeritics 3Flex system. Prior to analysis, each sample was dried at 60 °C in a vacuum oven and then degassed for 30 min at 90 °C and for 24 h at 200 °C. X-ray photoelectron spectroscopy (XPS) was conducted using an AXIS NOVA (KRATOS) with 150 W monochromatic Al-Kα radiation. Time-of-flight secondary ion mass spectrometry (ToF-SIMS) was conducted using TOF-SIMS5 (IONTOF).

### 2.3. Electrochemical characterization

A PIM-based carbon–sulfur composite electrode was fabricated using a dispersion of the active material, conducting carbon (Super P), and a polyvinylidene fluoride (PVdF) binder in a ratio of 8:1:1 in NMP. The slurry was cast on an aluminum current collector. Galvanostatic cycling was conducted at 167.5 mA $g^{-1}$ (1/10 C of the theoretical capacity of sulfur). The galvanostatic intermittent titration technique (GITT) was also applied with a current density of 167.5 mA $g^{-1}$ for every 5 minute with pauses until the dV/dt was lowered below 1 mV after 20 cycles for cycle stabilization. These were performed in a voltage range of 0.5–2.8 V (vs. $Na/Na^+$) using a TOSCAT–3100 (TOYO, Japan) and WBCS3000 (WonATech, Korea) battery testing systems at 30 °C. Electrochemical impedance spectroscopy (EIS) was conducted using an SP-150 potentiostat (BioLogic, France). For EIS analysis, each cell was cycled for 3 cycles and discharged to 1.0 V (vs. $Na/Na^+$) followed by a constant voltage until the current reached 10% of cycling. The tests were conducted using 2032 coin-type cells with a sodium metal (Sigma Aldrich) counter electrode, a glass fiber separator, and 1.0 M $NaClO_4$ in a mixture of ethylene carbonate (EC) and propylene carbonate (PC) (5:5 v:v).

## 3. Results and discussion

To prepare intrinsically microporous TB polymer-based carbon–sulfur composites, PIM-EA-TB was synthesized and used as a polymeric precursor, which is a shape-persistent ladder polymer consisting of EA and TB groups [26,30]. Generally, polymers of intrinsic microporosity (PIMs) are known as a class of porous polymers that contain numerous micropores, which are originated from their rigid and contorted molecular structures [22]. Further, it is well-known that PIMs with more rigid chemical structure can produce higher free volume and surface area. For example, PIM-EA-TB lead to more free volume and higher surface area than ethanoanthracene (EA) and Tröger's base (TB) units of PIM-EA-TB are more rigid chemical structure than SBI and benzodioxane of PIM-1 (Fig. 1). [26]. Specifically, the rigid backbones of the PIM-EA-TB result in inefficient packing, thereby producing a high free volume of 0.657 $cm^3\ g^{-1}$ and a higher surface area (1090 $m^2\ g^{-1}$) compared to that of PIM-1 (Table S1) [26,31]. Notably, benefiting from its high free volume, PIM-EA-TB can theoretically contain up to 55 wt% sulfur to the total weight of the carbon–sulfur composites. Although it is theoretical sulfur contents, this is higher value than 29 wt% of cPIMS-1-600 sample. In addition, PIM-EA-TB has a pore size of 0.6 nm with a narrow pore size distribution, and sulfur can be loaded as small sulfur allotropes in these pores. Also, the small sulfur molecules can react with crosslinking sites, such as methyl groups, aromatic rings, and TB groups, as in the case of PIM-1. Thus, PIM-EA-TB can be used as a polymeric precursor that can store small sulfur molecules and react with the sulfur molecules in their micropores, which result in the covalently bound small sulfur that can operate without the shuttle effect for room temperature Na–S batteries. It is noteworthy that extra sulfur molecules can be loaded in their larger free volume of PIM-EA-TB than that of PIM-1.

To confirm the actual sulfur content that can be loaded in the microporous materials, a series of cPIMS-EA-TB samples were prepared at different temperatures, as listed in Table S2. For comparison, the other carbon–sulfur composites were fabricated using PIM-1 or PIM-SBI-TB under the same temperature conditions, as listed in Table S2. All the composites were prepared through a one-step heat treatment of a mixture of sulfur and polymeric precursors. Each sample is referred to as cPIMS-EA-TB-X, cPIMS-1-X, or cPIMS-SBI-TB-X, where "c" represents the sample after carbonization, S indicates the samples that were reacted with sulfur, and X is the final temperature applied. For instance, cPIMS-EA-TB-600 was prepared through heat treatment of the mixture of sulfur and PIM-EA-TB at a final temperature of 600 °C. Also, cPIM-EA-TB-600 was heat treated PIM-EA-TB samples without sulfur molecules at a final temperature of 600 °C, which means that the sample contained no sulfur molecules. In the case of cPIMS-EA-TB-300, the carbon–sulfur composite contained 56 wt% of sulfur, and notably, the sulfur content is the theoretical maximum that can be stored in the free volume of PIM-EA-TB. This result is different from those previously reported for PIM-1 based carbon–sulfur composites, where the sulfur content of PIM-1 did not exceed 30 wt% [21]. This difference can be attributed to the higher free volume of PIM-EA-TB, which renders the sulfur molecules easily accessible to inner pores through more interconnected void spaces [32]. Further, the PIM-EA-TB-based carbon–sulfur composites had a higher sulfur content than other PIMs such as PIM-1 and PIM-SBI-TB after thermal treatment at a temperature range of 300–600 °C, as listed in Table S2. In addition, the sulfur molecules can be connected to the carbon matrix through the formation of covalent bonds during further heat treatments. The formation of covalent bonds between the sulfur molecules and the carbon matrix in the cPIMS-EA-TB series is supported by the results of TGA and XPS (Figs. S1 and S2). First, from the TGA curves, it is evident that free sulfur molecules and physically confined small sulfur were absent from 220 to 320 °C and from 300 to 480 °C, respectively, and there remained no residual sulfur molecules on the cPIMS-EA-TB series [33]. Furthermore, chemically bound sulfur molecules existed because there was no decomposition before 500 °C, and a single decomposition occurred above 500 °C for the cPIMS-EA-TB series [20]. Second, it is well-known that XPS experiment reveals the presence of C–S bonds. As illustrated in Fig. S2, the S 2p spectrum of the cPIMS-EA-TB 400, 500, and 600 samples showed a characteristic S $2p_{3/2}/2p_{1/2}$ doublet, which was separated by 1.2 eV with an intensity ratio of approximately 2:1, and where the S $2p_{3/2}$ peak (163.9 eV) had a relatively low binding energy than elemental sulfur (164.0 eV), which also meant the presence of C–S bonds [34–36]. Consequently, we confirmed that the sulfur molecules were covalently linked to the carbon matrix during heat treatment.

Therefore, the cPIMS-EA-TB series contained more sulfur molecules than those of the PIM-1-based carbon–sulfur composites, wherein the sulfur molecules are covalently bound to the carbon matrix.

A series of the as-prepared cPIMS-EA-TB samples were subjected to galvanostatic cycling to evaluate their electrochemical performance. As shown in Fig. 2, the first discharge capacity of the samples increased with heat treatment at temperatures up to 500 °C and then decreased with a further increase in the temperature. In addition, the samples treated at temperatures under 500 °C demonstrated acute capacity fading. In the case of cPIMS-EA-TB-300 sample, it showed negligible capacity and acute capacity fading. This is because carbon substrate was not synthesized properly due to low temperature. In the case of cPIMS-EA-TB-400 and cPIMS-EA-TB-500 sample, they delivered large capacity at first cycle and showed acute fading. The large irreversible capacity might come from carbon substrate, which is famous in sodium storage in carbon [37,38]. Acute capacity fading after 2nd cycles might come from insufficient conductivity. On the other hand, cPIMS-EA-TB-600 exhibited reversible cycling and negligible capacity fading after 2nd cycle. The irreversible capacity at 1st cycle came from carbon substrate, which is demonstrated by galvanostatic cycling of carbon substrate cPIM-EA-TB-600 without sulfur in Fig. S3. It delivered ca. 275 mA h $g^{-1}$ at 1st cycle and it was decreased to 75 mA h $g^{-1}$ after 2nd cycle (Fig. S3). The cycle performance difference among cPIMS-EA-TB samples indicates that electrical and ionic conductivity of electrode materials varies with temperature. The voltage profiles of cPIMS-EA-TB-600 are similar to that of cPIMS-1-600 based electrode that we reported before. It indicates that cPIMS-EA-TB-600 reacts with sodium through the same reaction mechanism as cPIMS-1-600, which utilizes covalently bound

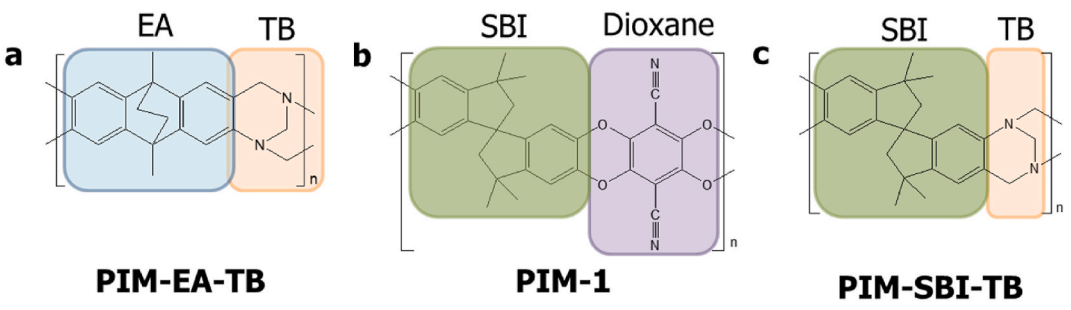


**Fig. 1.** Chemical structure of (a) PIM-EA-TB, (b) PIM-1, and (c) PIM-SBI-TB.

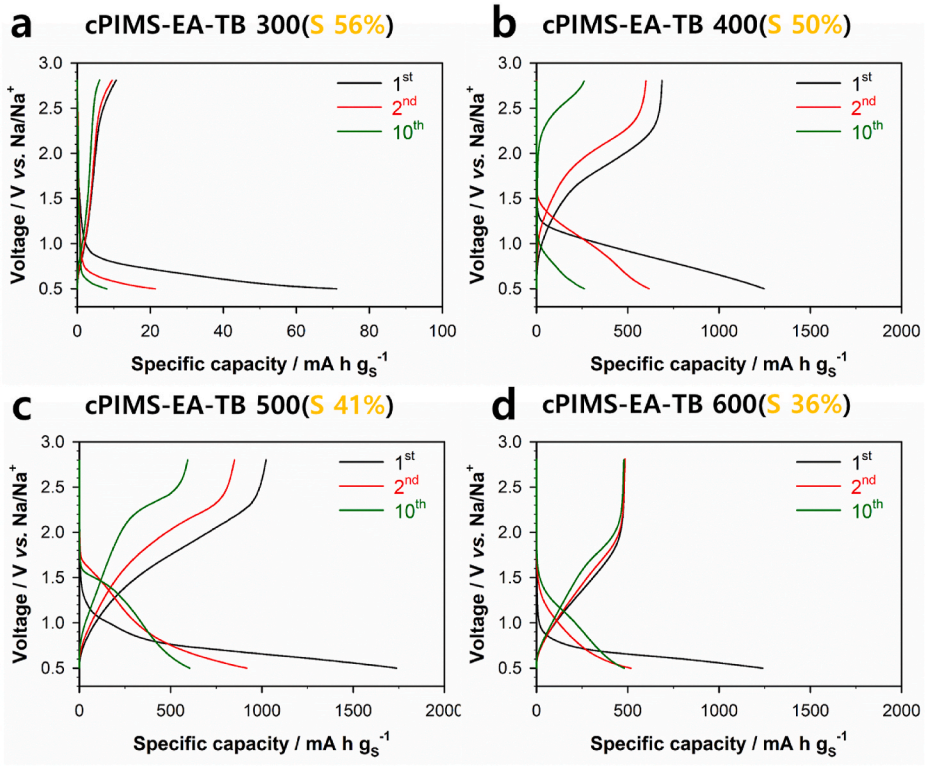


**Fig. 2.** Voltage profiles of cPIMS-EA-TB carbon–sulfur composites treated at different temperatures.

small sulfur in microporous carbons.

The conductivity difference is supported by the EIS results shown in Fig. S4. The samples were cycled for 3 cycles followed by a constant voltage of 1.0 V, which is the middle state of cycling containing both sodiated sulfur and non-sodiated sulfur. The samples treated at temperatures below 500 °C exhibited a larger charge transfer resistance than those treated at 600 °C. This indicates that the large resistance of the samples treated at temperatures below 500 °C hinders the reaction of composite sulfur with sodium. Furthermore, this is supported by the GITT results shown in Fig. S5. The samples treated at temperatures below 500 °C showed a larger overpotential than those treated at temperatures above 500 °C. This indicates that the samples treated at temperatures below 500 °C underwent higher resistance than that of cPIMS-EA-TB-600 during cycling. That is, the cPIMS-EA-TB-600 have higher conductivity than other cPIMS-EA-TB treated at temperatures below 500 °C.

The enhancement in electrical conductivity through high-temperature heat treatment can be attributed to the structural changes of the polymeric precursor. According to Rong et al., PIM-EA-TB undergoes stepwise degradation during thermolysis [39]. The steps comprised ethylene and methane loss, crosslinking, and degradation of the main chain, thereby resulting in the conversion of the polymeric precursor into $sp^2$ hybridized carbon. These changes in the chemical structure were scrutinized by performing a CP-MAS $^{13}C$ NMR analysis on cPIM-EA-TB fabricated under different heat treatment temperatures (Fig. 3). First, the pristine PIM-EA-TB contained methylene ($\delta = 20.32$ ppm), EA ($\delta = 38.66$ and 43.50 ppm), TB ($\delta = 61.44$ and 69.20 ppm), and aromatic units ($\delta = 119.91$, 127.04, and 147.69 ppm). After heat treatment at 400 °C, the TB units were decomposed, and a few EA units were diminished. Most of the methylene, EA, and TB groups were lost at 500 °C. Finally, further carbonization at 600 °C resulted in the decomposition of all the peaks of the PIMs, except for the $sp^2$ carbon peaks centered at 128.41 ppm. Thus, the PIM-EA-TB was converted to $sp^2$ hybridized carbon during this carbonization process, and the increase in the $sp^2$ carbon content led to the improvement in the electrical conductivity of the resulting PIM-EA-TB-based carbon [40]. Additionally, this structural variation was supported by Raman spectroscopy and XRD analysis (Figs. 4c, 4d, and S6).

Among the PIM-EA-TB-based carbon–sulfur composites, cPIMS-EA-TB-600 exhibited shuttle-free phenomenon similar to that of PIM-1-based carbon–sulfur composites, although the former cPIMS-EA-TB-300 has a higher sulfur content (56 wt%) than the latter cPIMS-EA-TB-600. Accordingly, focusing on the structural properties, including microporosity and covalent bonding, of the cPIMS-EA-TB-600, we further examined the electrochemical properties of the as-fabricated Na–S batteries.

First, as shown in the SEM and TEM images (Figs. 5 and S7), the sulfur molecules of cPIMS-EA-TB-600 were confirmed as being evenly distributed in the carbon–sulfur composites. Furthermore, the SEM and TEM images revealed that the sulfur molecules were evenly distributed without the agglomeration of sulfur throughout the carbon matrix. FIB-SEM images (Figs. S8 and S9) also showed the sulfur molecules are well distributed on the surface and inside of the sample as suggested by Fig. 5a. Second, argon adsorption tests revealed that the evenly distributed sulfur molecules were confined in micropores with a pore size of approximately 0.6 nm (Fig. 4a and b). To scrutinize the pore structure of the carbonized PIM-EA-TB, cPIM-EA-TB-600 was prepared by carbonizing the PIM-EA-TB without elemental sulfur at 600 °C because it was difficult to observe the characteristics of the pores of cPIMS-EA-TB-600, which were filled with sulfur molecules. cPIM-EA-TB-600 had a specific surface area of 374 $m^2\ g^{-1}$ and exhibited a type I isotherm, indicating that they consist of micropores (Table S1 and Fig. 4a). Further, the Horvath–Kawazoe (H–K) plots (Fig. 4b) reveal that the micropores were approximately 0.6 nm in size with a narrow pore size distribution, wherein the sulfur molecules can exist as smaller sulfur ($S_{2\text{-}4}$) allotropes under spatial constraints [19]. Moreover, cPIMS-EA-TB-600 possessed a low specific surface area of 6.56 $m^2\ g^{-1}$ because they were filled with sulfur molecules. Additionally, XRD analysis revealed that the sulfur molecules did not exist as large elemental sulfur ($S_8$), wherein elemental sulfur ($S_8$) has an orthorhombic

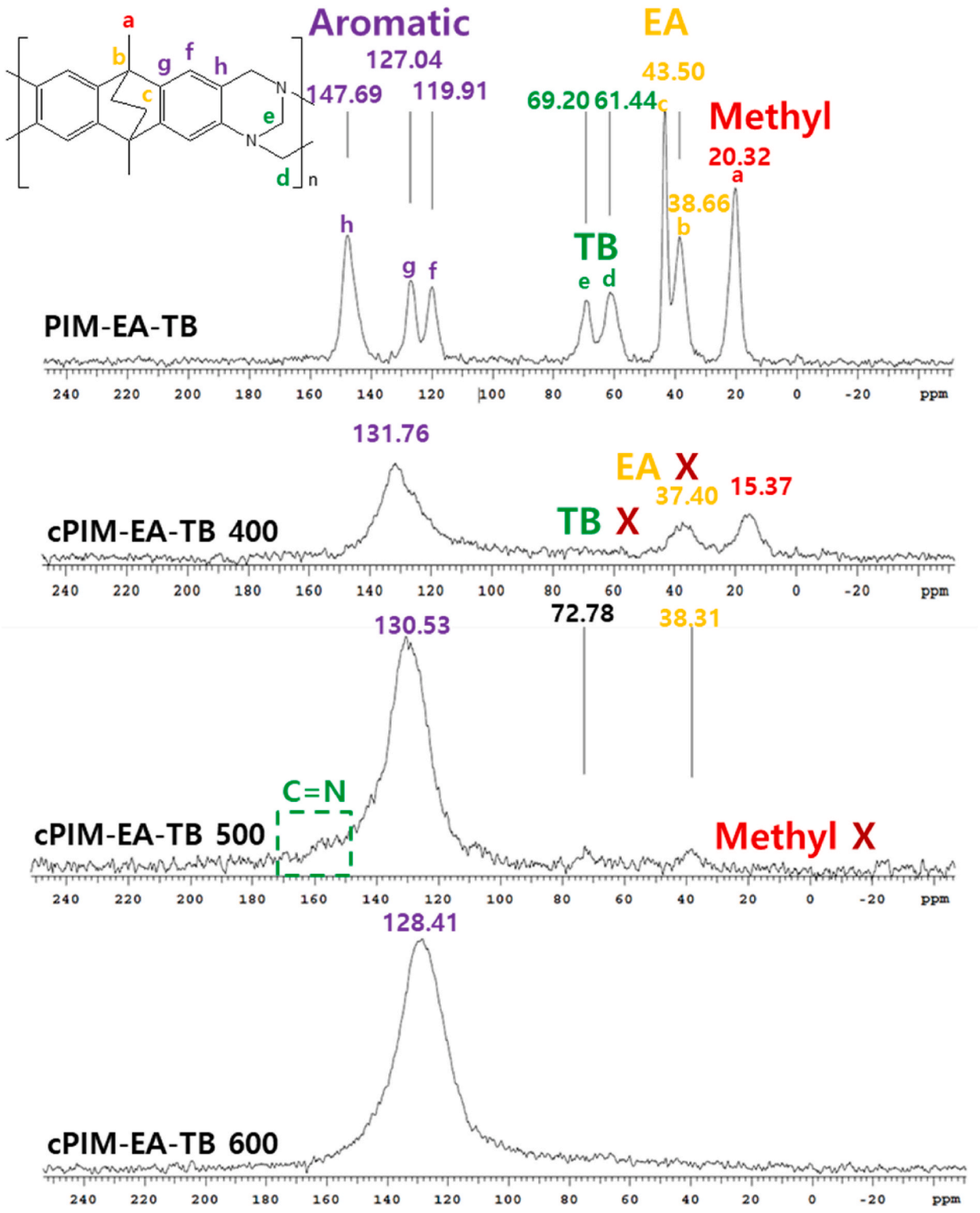


**Fig. 3.** $^{13}C$ CP-MAS NMR analysis for a series of cPIM-EA-TB samples treated at different temperatures.

structure with the (222), (026), and (040) planes, which correspond to 23.1, 25.9, and 27.8°, respectively.

Lastly, the covalent bonding between the smaller sulfur molecules and the carbon matrix was corroborated by ToF-SIMS analysis. CNS fragments (i.e., $CNS^-$ at $m/z = 58$, $C_3NS^-$ at $m/z = 82$, and $C_5NS^-$ at $m/z = 106$), CS fragments (i.e., $CS^-$ at $m/z = 44$ and $C_2S^-$ at $m/z = 56$), an SN fragment ($SN^-$ at $m/z = 46$), and an oligo-sulfide structure (i.e., $S_3^-$ at $m/z = 96$) were detected via ToF-SIMS, indicating that small sulfur molecules in cPIMS-EA-TB-600 were linked to the carbon matrix [41]. In addition, the XPS spectra of cPIMS-EA-TB-600 reconfirmed the presence of C–S bonds (Figs. S2e and f). In the S 2p spectrum, the characteristic S $2p_{3/2}$ and $2p_{1/2}$ doublet were found with an energy separation of 1.2 eV and an intensity ratio of approximately 2:1. Moreover, the S $2p_{3/2}$ (163.9 eV) peak has a lower binding energy than that of elemental sulfur (164.0 eV). Accordingly, the prepared cPIMS-EA-TB-600 contained covalently bound small sulfur molecules in its micropores, thereby obstructing the dissolution of sulfur from the carbon–sulfur matrix.

Owing to these aspects, cPIMS-EA-TB-600 showed stable cycle

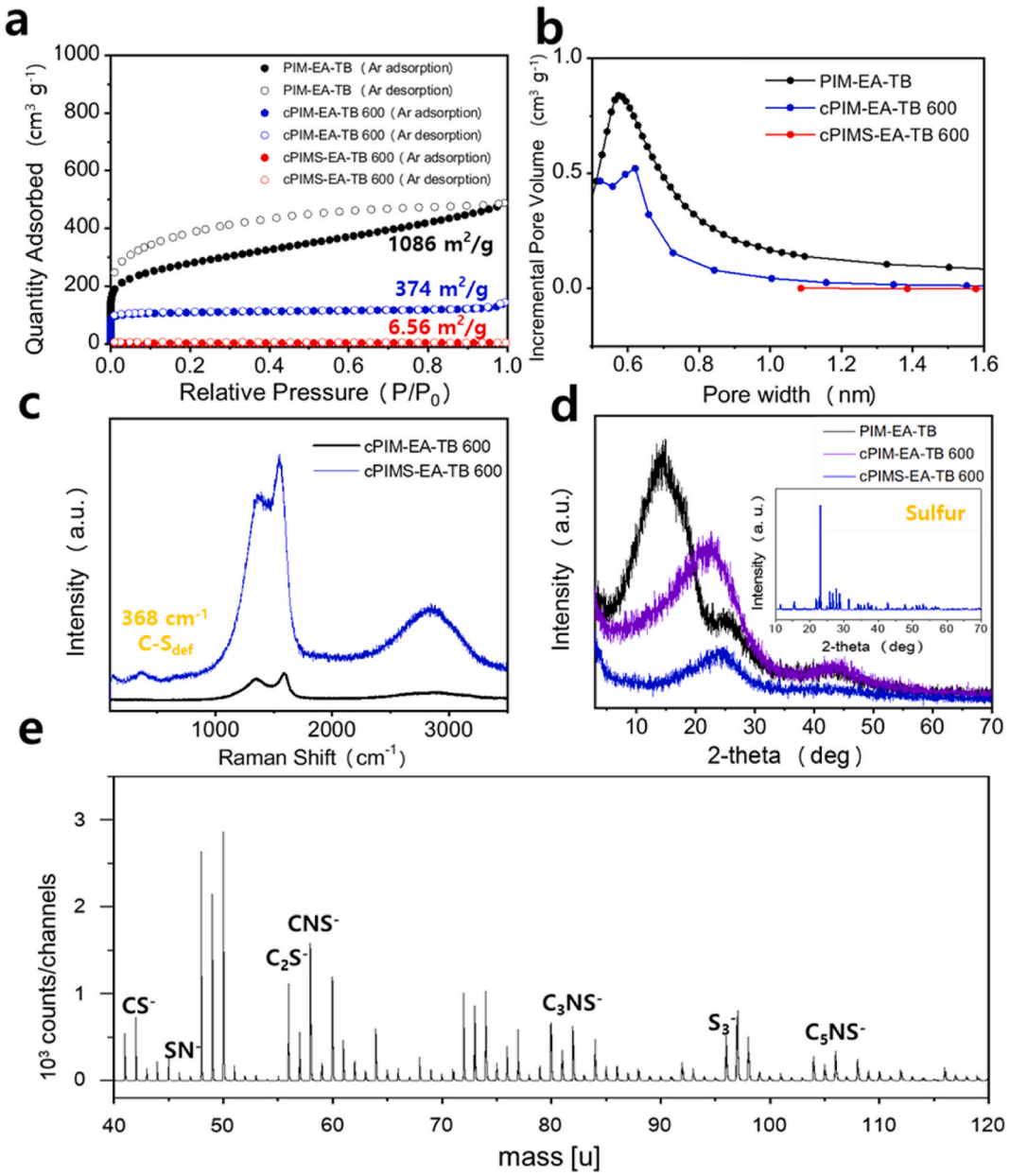


**Fig. 4.** (a) Ar adsorption/desorption isotherms, (b) pore size distribution plots, (c) Raman spectra, and (d) XRD patterns of cPIM-EA-TB-600 and cPIMS-EA-TB-600, and (e) ToF-SIMS spectrum of cPIMS-EA-TB-600.

performance when utilized as a Na–S battery cathode, as shown in Fig. 6. It exhibited a high reversible capacity of approximately 500 mA h $g^{-1}$ after stabilization and maintained a stable cycle over 350 cycles. In addition, it exhibited a high coulombic efficiency (approximately greater than 99%), implying that it effectively prevented the side reactions of sodium polysulfide and shuttle effect. This high coulombic efficiency can be attributed to the fact that the covalently bound small sulfur molecules of cPIMS-EA-TB-600 did not diffuse into the electrolyte during cycling. The reaction mechanism of cPIMS-EA-TB-600 was also confirmed by dQ/dV plot of 100th cycle (Fig. S10), where one redox couple appeared at 1.14 V during discharge and 1.85 V during charge and there was no evidence on re-oxidation to elemental sulfur that occurs near 2.2 V [3,41]. Further, it was revealed that there was no sulfur dissolution by observing difference in UV–Vis spectra for both samples of cPIMS-EA-TB-600 only stored in coin cell and one cycled for 10 cycles (Fig. S11). It means cPIMS-EA-TB-600 can suppress sulfur dissolution during cycling. The characteristics during cycling were illustrated in Fig. S12. In addition, it showed improved rate performance compared to cPIMS-1-600 that we reported before as shown in Figs. S13 and S14. Thus, cPIMS-EA-TB-600 can be used as a promising cathode material for RT Na–S batteries without the shuttle effect.

## 4. Conclusions

Herein, the highly porous polymeric precursor PIM-EA-TB was used to fabricate carbon–sulfur composites for shuttle-effect-free RT Na–S batteries. After being subjected to heat treatment, the PIM-EA-TB-based carbon–sulfur composites contained more sulfur owing to their large free volume. cPIMS-EA-TB-600 possessed 36 wt% of sulfur molecules, which is higher than that previously reported for PIM-1. In addition, benefiting from the characteristics of PIM, the PIM-EA-TB-based carbon–sulfur composites can operate without the shuttle effect because they contain small sulfur molecules in their micropores, and these molecules are covalently linked with the carbon matrix. Additionally,

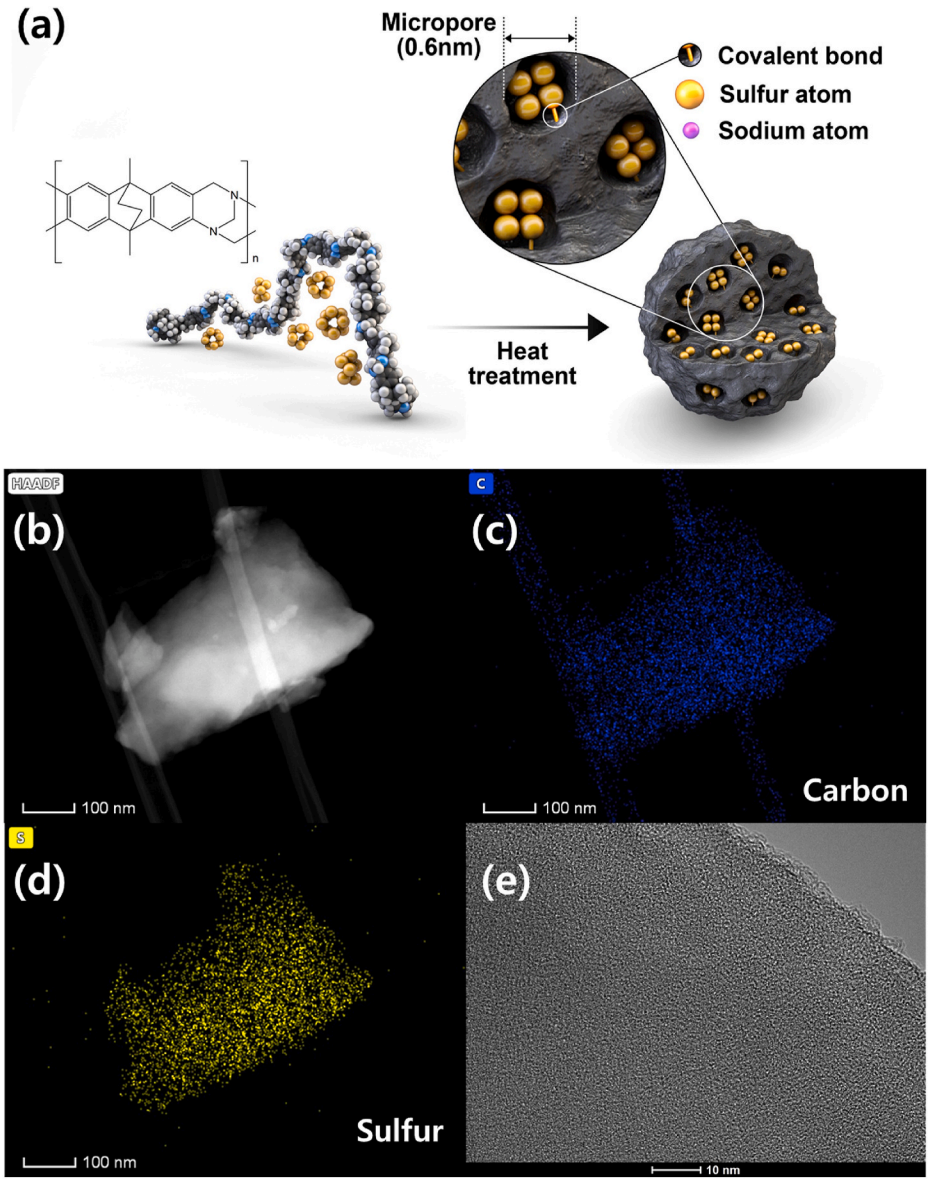


**Fig. 5.** (a) Schematic of the preparation procedure of PIM-EA-TB-based carbon–sulfur composites, (b) high-angle annular dark-field STEM image of cPIMS-EA-TB-600, (c) elemental mapping of carbon, (d) elemental mapping of sulfur, and (e) high-resolution TEM image.

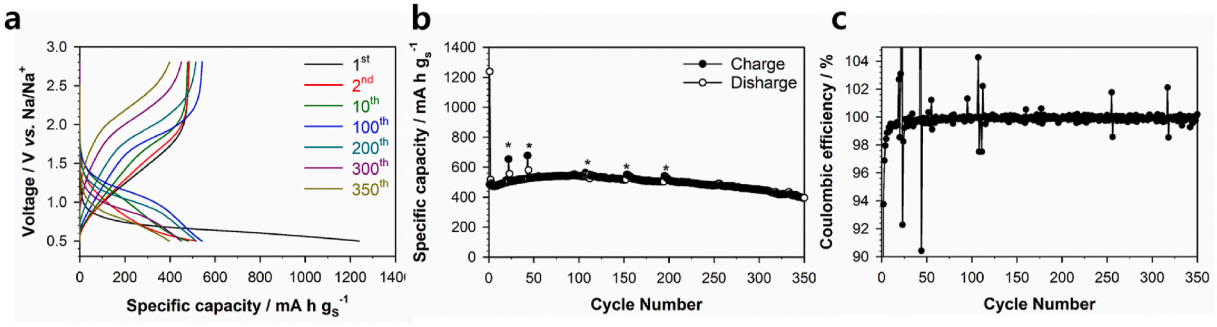


**Fig. 6.** Electrochemical properties of cPIMS-EA-TB-600 composites. (a) Voltage profiles of cPIMS-EA-TB-600, (b) specific capacity and (c) coulombic efficiencies versus the cycle number of cPIMS-EA-TB-600. *Unusual points in cycle performance and coulombic efficiency within 50 cycles and after 100 cycles were due to the instability of Na metal and the electrical shutdown of the cycler, respectively.

after the heat treatment, the PIM-EA-TB was converted into an electrically conductive carbon matrix, which complemented the insulating nature of the sulfur molecules. Furthermore, the electrochemical tests revealed a high reversible capacity of approximately 500 mA h $g^{-1}$ after stabilization and the composite maintained a stable cycle over 350 cycles with high coulombic efficiency (approximately greater than 99%).

Consequently, we propose that PIMs with higher free volumes, such as PIM-EA-TB, can be used as polymeric precursors that can enable the realization of the ideal cathode materials for shuttle-effect-free Na–S batteries.

## CRediT authorship contribution statement

**Jun Woo Jeon:** Conceptualization, Writing – original draft, Writing – review & editing, Data curation, Resources. **Dong-Min Kim:** Writing – original draft, Resources, Methodology, Visualization. **Jinyoung Lee:** Investigation, Resources, Formal analysis. **Min Su Kim:** Investigation, Formal analysis. **Min Ho Jeon:** Investigation, Formal analysis. **Richard Malpass-Evans:** Validation, Resources. **Neil B. McKeown:** Validation, Writing – review & editing. **Kyu Tae Lee:** Supervision, Project administration, Funding acquisition, Writing – review & editing. **Byoung Gak Kim:** Supervision, Funding acquisition, Project administration, Writing – review & editing.

## Declaration of competing interest

The authors declare that they have no known competing financial interests or personal relationships that could have appeared to influence the work reported in this paper.

## Acknowledgment

J. W. Jeon and D.-M. Kim contributed equally to this work.

## Appendix A. Supplementary data

Supplementary data to this article can be found online at https://doi.org/10.1016/j.jpowsour.2021.230539.

## Funding

This work was supported by the Korea Research Institute of Chemical Technology (KRICT) core project [grant numbers SI2121-20 and BSF20-242].

## References

[1] Y.X. Wang, W.H. Lai, S.L. Chou, H.K. Liu, S.X. Dou, Adv. Mater. 32 (2020) 1903952.
[2] Y.X. Wang, B. Zhang, W. Lai, Y. Xu, S.L. Chou, H.K. Liu, S.X. Dou, Adv. Energy Mater. 7 (2017) 1602829.
[3] A. Manthiram, X. Yu, Small 11 (2015) 2108–2114.
[4] N. Wang, Y. Wang, Z. Bai, Z. Fang, X. Zhang, Z. Xu, Y. Ding, X. Xu, Y. Du, S. Dou, Energy Environ. Sci. 13 (2020) 562–570.
[5] Y.X. Wang, W.H. Lai, Y.X. Wang, S.L. Chou, X. Ai, H. Yang, Y. Cao, Angew. Chem. Int. Ed. 58 (2019) 18324–18337.
[6] S. Xin, L. Gu, N.-H. Zhao, Y.-X. Yin, L.-J. Zhou, Y.-G. Guo, L.-J. Wan, J. Am. Chem. Soc. 134 (2012) 18510–18513.
[7] M. Kohl, F. Borrmann, H. Althues, S. Kaskel, Adv. Energy Mater. 6 (2016) 1502185.
[8] Q. Pang, X. Liang, C.Y. Kwok, L.F. Nazar, Nat. Energy 1 (2016) 16132.
[9] C.-W. Park, H.-S. Ryu, K.-W. Kim, J.-H. Ahn, J.-Y. Lee, H.-J. Ahn, J. Power Sources 165 (2007) 450–454.
[10] C. Li, A.L. Ward, S.E. Doris, T.A. Pascal, D. Prendergast, B.A. Helms, Nano Lett. 15 (2015) 5724–5729.
[11] S. Duangdangchote, A. Krittayavathananon, N. Phattharasupakun, M. Sawangphruk, ECS Trans 97 (2020) 827.
[12] S. Wei, S. Xu, A. Agrawral, S. Choudhury, Y. Lu, Z. Tu, L. Ma, L.A. Archer, Nat. Commun. 7 (2016) 11722.
[13] Y. Hu, R. Han, L. Mei, J. Liu, J. Sun, K. Yang, J. Zhao, Mater. Today Energy (2020) 100608.
[14] C. Chen, Q. Jiang, H. Xu, Y. Zhang, B. Zhang, Z. Zhang, Z. Lin, S. Zhang, Nanomater. Energy 76 (2020) 105033.
[15] H. Chen, Z. Wu, Z. Su, L. Hencz, S. Chen, C. Yan, S. Zhang, J. Energy Chem. 62 (2021) 127–135.
[16] T. Li, J. Xu, C. Wang, W. Wu, D. Su, G. Wang, J. Alloys Compd. 792 (2019) 797–817.
[17] L. Hencz, H. Chen, H.Y. Ling, Y. Wang, C. Lai, H. Zhao, S. Zhang, Nano-Micro Lett. 11 (2019) 1–44.
[18] X. Gu, Y. Wang, C. Lai, J. Qiu, S. Li, Y. Hou, W. Martens, N. Mahmood, S. Zhang, Nano Res 8 (2015) 129–139.
[19] S. Xin, Y.X. Yin, Y.G. Guo, L.J. Wan, Adv. Mater. 26 (2014) 1261–1265.
[20] T.H. Hwang, D.S. Jung, J.-S. Kim, B.G. Kim, J.W. Choi, Nano Lett. 13 (2013) 4532–4538.
[21] J.W. Jeon, D.-M. Kim, J. Lee, J.-C. Lee, Y.S. Kim, K.T. Lee, B.G. Kim, J. Mater. Chem. 8 (2020) 3580–3585.
[22] P.M. Budd, B.S. Ghanem, S. Makhseed, N.B. McKeown, K.J. Msayib, C. E. Tattershall, Chem. Commun. (2004) 230–231.
[23] Y. Wang, D. Zhou, V. Palomares, D. Shanmukaraj, B. Sun, X. Tang, C. Wang, M. Armand, T. Rojo, G. Wang, Energy Environ. Sci. 13 (2020) 3848–3879.
[24] J. Gao, M.A. Lowe, Y. Kiya, H.c.D. Abruña, J. Phys. Chem. C 115 (2011) 25132–25137.
[25] J.W. Jeon, D.-G. Kim, E.-h. Sohn, Y. Yoo, Y.S. Kim, B.G. Kim, J.-C. Lee, Macromolecules 50 (2017) 8019–8027.
[26] M. Carta, R. Malpass-Evans, M. Croad, Y. Rogan, J.C. Jansen, P. Bernardo, F. Bazzarelli, N.B. McKeown, Science 339 (2013) 303–307.
[27] R. Williams, L.A. Burt, E. Esposito, J.C. Jansen, E. Tocci, C. Rizzuto, M. Lanč, M. Carta, N.B. McKeown, J. Mater. Chem. 6 (2018) 5661–5667.
[28] H. Shamsipur, B.A. Dawood, P.M. Budd, P. Bernardo, G. Clarizia, J.C. Jansen, Macromolecules 47 (2014) 5595–5606.
[29] J.W. Jeon, J. Shin, J. Lee, J.-H. Baik, R. Malpass-Evans, N.B. McKeown, T.-H. Kim, J.-C. Lee, S.-K. Kim, B.G. Kim, Appl. Surf. Sci. 530 (2020) 147146.
[30] G. Maier, Angew. Chem. Int. Ed. 52 (2013) 4982–4984.
[31] H. Yin, B. Yang, Y.Z. Chua, P. Szymoniak, M. Carta, R. Malpass-Evans, N. B. McKeown, W.J. Harrison, P.M. Budd, C. Schick, ACS Macro Lett. 8 (2019) 1022–1028.
[32] X. Chen, Z. Zhang, L. Wu, X. Liu, S. Xu, J.E. Efome, X. Zhang, N. Li, ACS Appl. Polym. Mater. 2 (2020) 987–995.
[33] T. Takahashi, M. Yamagata, M. Ishikawa, Prog. Nat. Sci.: Met. Mater. Int. 25 (2015) 612–621.
[34] G. Li, J. Sun, W. Hou, S. Jiang, Y. Huang, J. Geng, Nat. Commun. 7 (2016) 10601.
[35] Z. Wang, Y. Dong, H. Li, Z. Zhao, H.B. Wu, C. Hao, S. Liu, J. Qiu, X.W.D. Lou, Nat. Commun. 5 (2014) 5002.
[36] C. Zu, A. Manthiram, Adv. Energy Mater. 3 (2013) 1008–1012.
[37] Z. Li, C. Bommier, Z.S. Chong, Z. Jian, T.W. Surta, X. Wang, Z. Xing, J. C. Neuefeind, W.F. Stickle, M. Dolgos, P.A. Greaney, X. Ji, Adv. Energy Mater. 7 (2017) 1602894.
[38] Y. Wang, Y. Zhang, H. Cheng, Z. Ni, Y. Wang, G. Xia, X. Li, X. Zeng, Molecules 26 (2021) 1535.
[39] Y. Rong, D. He, A. Sanchez-Fernandez, C. Evans, K.J. Edler, R. Malpass-Evans, M. Carta, N.B. McKeown, T.J. Clarke, S.H. Taylor, Langmuir 31 (2015) 12300–12306.
[40] Y. Lin, Z. Feng, L. Yu, Q. Gu, S. Wu, D.S. Su, Chem. Commun. 53 (2017) 4834–4837.
[41] J. Fanous, M. Wegner, J. Grimminger, A.n. Andresen, M.R. Buchmeiser, Chem. Mater. 23 (2011) 5024–5028.

## Glossary

*TB:* Tröger's base
*PIM:* polymer of intrinsic microporosity
*EA:* ethanoanthracene
*EIS:* electrochemical impedance spectroscopy
*SBI:* spirobisindane